Bacteriocin AS-48 binding to model membranes and pore formation as revealed by coarse-grained simulations

Cruz, Victor L.; Ramos, Javier; Martinez-Salazar, Javier; Melo, Manuel N.

Published in:
Biochimica et Biophysica Acta-Biomembranes

DOI:
10.1016/j.bbamem.2013.05.036

Publication date:
2013

Biochimica et Biophysica Acta 1828 (2013) 2524–2531

Contents lists available at ScienceDirect

Biochimica et Biophysica Acta

journal homepage: www.elsevier.com/locate/bbamem

Bacteriocin AS-48 binding to model membranes and pore formation as revealed by coarse-grained simulations

Victor L. Cruz [a,*], Javier Ramos [a], Manuel N. Melo [b], Javier Martinez-Salazar [a]

[a] BIOPHYM, Instituto de Estructura de la Materia CSIC, Serrano-113-bis., 28006 Madrid, Spain
[b] Groningen Biomolecular Sciences and Biotechnology Institute and Zernike Institute for Advanced Materials, University of Groningen, Nijenborgh 7, 9747 AG Groningen, The Netherlands

ARTICLE INFO

Article history:
Received 1 September 2012
Received in revised form 24 May 2013
Accepted 31 May 2013
Available online 10 June 2013

Keywords:
AS-48 bacteriocin
Coarse-grained simulation
Antimicrobial peptide

ABSTRACT

Bacteriocin AS-48 is a membrane-interacting peptide that acts as a broad-spectrum antimicrobial against Gram-positive and Gram-negative bacteria. Prior Nuclear Magnetic Resonance experiments and the high resolution crystal structure of AS-48 have suggested a mechanism for the molecular activity of AS-48 whereby the peptide undergoes transition from a water-soluble to a membrane-bound state upon membrane binding. To help interpret experimental results, we here simulate the molecular dynamics of this binding mechanism at the coarse-grained level. By simulating the self-assembly of the peptide, we predict induction by the bacteriocin of different pore types consistent with a "leaky slit" model.

1. Introduction

Antimicrobial peptides (AMP) have a number of interesting properties that make them promising candidates for the treatment of infectious diseases and food preservation. Their mechanisms of action have been addressed in several experimental and simulation studies [1–21]. These studies have revealed, for example, that by having several mechanisms of enzyme inhibition, some AMPs are able to avoid the development of microbial resistance. In recent reviews of the structure and properties of AMPs [4,14], cyclic peptides in particular emerged as a special class of very stable active compounds [13].

In the late 1980s, AS-48, a cyclic 70-residue peptide showing remarkable stability and bactericidal activity, was isolated from bacteria by Galvez, Valdivia, Maqueda and coworkers [22–24]. Ten years later, NMR and X-ray crystallography revealed the dimeric structure of this bacteriocin [25–27]. The monomer (aka protomer) is composed of five alpha-helices enclosing a hydrophobic core in a compact globular structure (see Fig. 1). It is accepted that charged residues are mainly located in the α_4 and α_5 helices separate from the hydrophobic regions. Four negatively charged GLU residues form a patch that segregates the hydrophobic zone from an area of positively charged residues (blue regions in α_4 and α_5).

In aqueous solution, AS-48 peptides appear as dimeric form I or II (PDB ID: 1O83 and 1O84, respectively) depending on the chemical environment. Protomers arrange themselves in such a way that hydrophobic residues are buried in the dimer peptide core while charged residues interact with the surrounding water environment (see Fig. 2.a). When a detergent is added, the dimer adopts a contiguous organisation such that the hydrophobic moiety of each protomer remains in the hydrophobic phase while charged residues occupy the water phase (see Fig. 2.b).

According to this behaviour, it has been hypothesized [27] that, in solution, AS-48 adopts the configuration of dimeric form I and switches to dimeric form II upon binding to the bacterial membrane (see Fig. 4 in ref [27]). This transition implies a 90° rotation of each protomer within dimer I allowing the dimer to insert in the membrane. This exposes the hydrophobic peptide surface to the hydrophobic lipid tails whereas charged areas interact with the charged phospholipid head groups. Unfortunately, direct experimental support for this hypothesis is lacking.

A further hypothesis based on the results of electrochemical experiments proposes that the bacteriocin is able to form membrane pores some 7 Å in diameter [28].

Bacteriocin AS-48 selectively attacks bacterial membranes [29,30]. This observation is consistent with the general trend noted for some antimicrobial peptides and has been nicely illustrated by in vitro experiments using model membranes [31–33]. Bacterial membranes feature high proportions of anionic lipids such as dipalmitoyl posphatidyl glycerol (DPPG) or dipalmitoyl phosphatidic acid (DPPA) [34,35]. Experiments performed on AS-48 and DPPA monolayers have revealed that only at pH > 10 does energetically favourable interaction between these monolayers occur, but at the expense of substantial modification to the secondary structure of AS-48 [36]. This finding, however, contrasts sharply with the increased bactericidal effect detected at pH values between 4 and 8 in bioactivity experiments [37].

A number of experiments using engineered AS-48 derivatives have sought to identify the main amino acids responsible for the bioactivity

* Corresponding author. Tel.: +34 915616800.
E-mail address: victor.cruz@iem.cfmac.csic.es (V.L. Cruz).

0005-2736/$ – see front matter © 2013 Elsevier B.V. All rights reserved.
http://dx.doi.org/10.1016/j.bbamem.2013.05.036

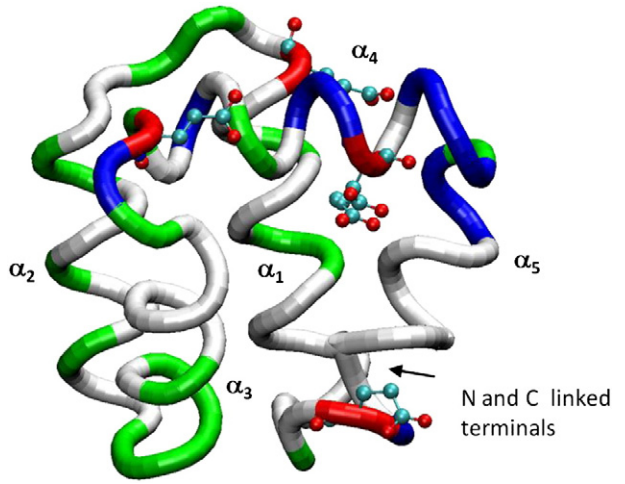

Fig. 1. Tube representation of the AS-48 protomer. Blue and red colours indicate positively and negatively charged residues, and green and white, polar and hydrophobic amino acids, respectively. Negatively-charged GLU resides are explicitly shown as the CPK model. The five helices α_1 to α_5 span residues 9–21, 25–34, 37–45, 51–62, and 64–5, respectively [26].

of this peptide [38–40]. The results of such studies indicate that wild type bacteriocin is the most active peptide [41].

The present study was designed to gain insight into the mechanism of action of bacteriocin AS-48 via a series of simulation experiments. For the simulations, we selected the MARTINI coarse-grained (CG) force field model since it is able to probe the spatial and time scales of systems beyond what is feasible using traditional all-atom models [42–44]. In effect, several studies have confirmed the consistency of different coarse-grained models used to simulate AMP systems and their interactions with lipid bilayers [6,45–50].

2. Computation methods

The starting structure for peptide dimer I was built directly from its X-ray structure (PDB ID: 1O83). For all the systems examined, the MARTINI CG force field model was used to map four atoms to one coarse-grained particle, i.e., four heavy atoms are represented by a single interaction centre [51,52]. DPPA lipid particles were similarly assigned to the DPPC molecule except that the particle associated with the choline group was removed leaving a net charge of −1 as the expected charge at physiological pH. Simulations were run in the NPT ensemble, coupling the system to a temperature and pressure bath according to the Berendsen coupling scheme [53]. The target temperature was 310 K and semi-isotropic pressure coupling was set to a reference pressure of 1 atm using a compressibility of 4.6×10^{-5} bar^{-1}. Lennard–Jones interactions were smoothly shifted to zero within the range of 0.9 and 1.2 nm and electrostatic interactions were also shifted to zero between 0 and 1.2 nm, according to recommendations for these coarse-grained simulations [48].

The total charge of the system was neutralized with 500 counter ions. Each protomer has a net charge of +6 and each DPPA lipid molecule has a −1 charge, as stated above.

The DPPA bilayer was built after the removal of choline particles from a previously equilibrated DPPC bilayer. This bilayer was duplicated in the X and Y directions, yielding a final system of 512 lipids. A water slab was added to the system to yield a Z dimension of 15.5 nm. This gives room for the later insertion of a peptide dimer, avoiding periodicity artefacts. The system was then equilibrated for 100 ns under the described conditions. In a subsequent step, the dimer was inserted in the water phase, and all water particles within 0.25 nm of any protein particle removed. The system was energy-minimized and then equilibrated using position restraints in protein pseudoatoms until lipid/protein, protein/water interaction energies had stabilized. In the next step, simulations of variable lengths were performed without further restraints. For systems with the protein inserted in the bilayer, the same procedure was applied. Protomers were placed in the selected position in the bilayer interior and lipid and water molecules within 0.25 nm of each protein particle were excluded from the model. Further details of the simulated systems are given below in the corresponding sections. The time-step used in all simulations was 0.03 ps, as recommended for MARTINI coarse-grained based simulations.

All calculations were performed using the GROMACS 4.5 package [54].

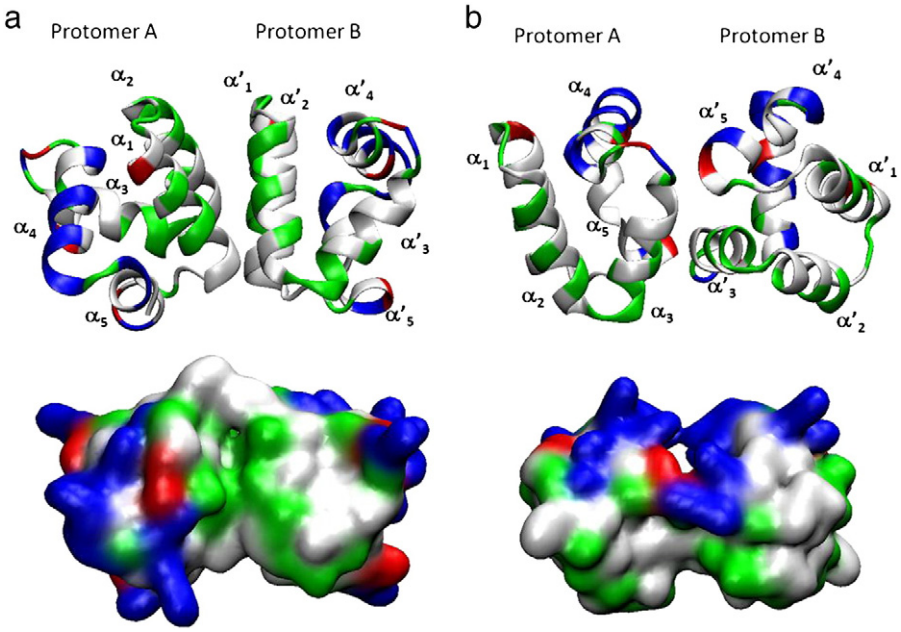

Fig. 2. The two dimeric forms of AS-48 indicated by crystallography. a: Dimeric form I (in aqueous solution, PDB ID: 1O83). b: Dimeric form II (in detergent, PDB ID: 1O84). Cartoon (top) and surface (bottom) representations in which the colours blue and red indicate positively and negatively charged residues, and green and white, polar and hydrophobic amino acids, respectively.

Elastic network formalism was used for each protomer to maintain the overall structure of the bacteriocin while preserving the internal flexibility inherent to the stability of this globular structure [55]. The network was built taking into account a cut-off of 0.9 nm with an elastic force constant of 500 kJ/mol.

Our use of elastic networks was justified by the relative rigidity of the AS-48 peptide structure observed in both X-ray and NMR experiments. We attribute the additional structural stability ascribed to this antimicrobial peptide to its α-helix packing and cyclic nature.

3. Results and discussion

3.1. Stability of AS-48 in solution

Coarse-grained simulation of dimeric form I of the peptide indicated a highly stable quaternary structure in water solution compared to its initial structure derived from crystallographic data. Fig. S1 (Supplementary Information) shows the rmsd of each protomer throughout the simulation, this value remaining constant from the start. The parameters selected for the elastic network seemed to guarantee the overall structure of each protomer. In Fig. 3, the structure of the dimer is illustrated after 3 μs. During simulation, the overall structure of the dimer was stable. Hydrophobic residues remained in the dimer centre shielded by polar and charged residues. In Fig. 3, the changes produced in distances between the centre of mass (COM) and the hydrophilic residues of both protomers may be observed, along with the COM distance between the respective hydrophobic domains. It may be noted that the dimer remains essentially stable during simulation with only a slight change detected at around 1 μs, presumably due to a small adjustment of hydrophobic interaction in the inner portion of the AS-48 dimer. We mapped the average minimum distance between residues of both protomers (Fig. S2) to assess their interactions. The figure shows that helices 2 and 3 of the first protomer interact with helices 1 and 2 of the second protomer. Helices 1 to 3 are rich in hydrophobic residues so are prone to interact either with the lipid acyl chains or with those helices in other protomers. Conversely, helices 4 and 5 contain charged LYS, ARG and GLU residues which tend to interact with lipid polar heads or the water solvent.

3.2. AS-48 dimer I binding to the lipid bilayer

The available experimental data indicate that AS-48 selectively binds to the bacterial membrane while it leaves normal Eucaryotic cell membranes intact [12]. The main difference between bacterial and Eucaryotic cytoplasmic membranes is the high proportion of anionic lipids in the former and abundant zwitterion species in the latter.

We simulated the binding process to two types of lipid bilayer, the first consisting of the anionic DPPA lipid and the other comprised of the zwitterion-neutral DPPC molecule. DPPA was modelled as a single negative charge at phosphate particles, corresponding to the ionization state of the lipid at a pH range of 3 to 9. In a 50 ns run, the AS-48 dimer was found to spontaneously bind to one of the DPPA layers (Fig. 4) and remained on the bilayer surface via separation of phosphate particles.

In contrast, no AS-48 dimer binding to the DPPC membrane was observed after 3 μs of simulation. Thus, the AS-48 dimer persisted in the water phase during the whole simulation period, as may be observed in Fig. 4. This finding is in line with the general observation that cationic AMPs do not seem to interact with zwitterionic bilayers, the major components of mammalian Eucaryotic cells [12].

Another model for an anionic lipid frequently used is the dipalmitoyl phosphatidyl glycerol DPPG bilayer. Following 4.5 μs simulations of AS-48 dimer binding to a DPPG bilayer, we observed similar behaviour to that noted for DPPA. Hence, the dimer was adsorbed onto the lipid surface without penetrating it. In Fig. 4, we provide the final snapshot of one of these simulations including the DPPG bilayer and the distance changes produced over time from the As-48 dimer COM to the bilayer centre.

The water model originally included in the MARTINI force field model used in our simulations does not consider electrostatic contributions. To determine the possible effects of electrostatic forces we replaced the water model with a polarisable water model described by Yesylevskyy [56]. The computational cost is around one order of magnitude over the cost of the non-polarisable water model. The results obtained are similar to those obtained using the original MARTINI water model. Thus, the AS-48 dimer approaches the bilayer surface and is adsorbed onto the surface without penetrating the bilayer interior within the simulation time. The main difference with the uncharged water model is that the approximation to the surface is delayed by the polarisable water, as can be observed in Fig. S3 (Supplementary Information). In this figure, the distance from the dimer COM to the bilayer centre is plotted against time illustrating that it takes close to 1.5 μs for one of the protomers to approach the lipid bilayer surface. The final snapshot of this simulation is shown in Fig. S3 and can be compared with the corresponding one for the non-polarisable water model system in Fig. 4.

Binding of AS-48 to an anionic lipid bilayer shows a complex potential energy landscape with non-negligible energy barriers between stable states. This could mean that the system is kinetically trapped in

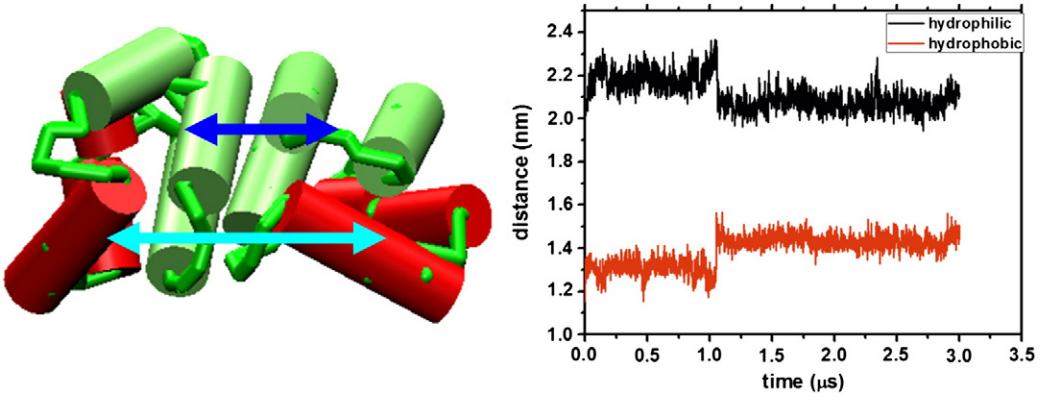

Fig. 3. AS-48 dimer in solution. Left: Structure of dimeric form I after 3 μs of MD simulation at the coarse-grained (CG) level. Green cylinders represent helices 1 to 3 (mostly hydrophobic) and red cylinders the hydrophilic helices 4 and 5. Blue and cyan arrows indicate distances between the centres of mass of hydrophobic and hydrophilic residues, respectively. Right: Changes produced in the distance between hydrophilic and hydrophobic residue centres of mass in both AS-48 protomers.

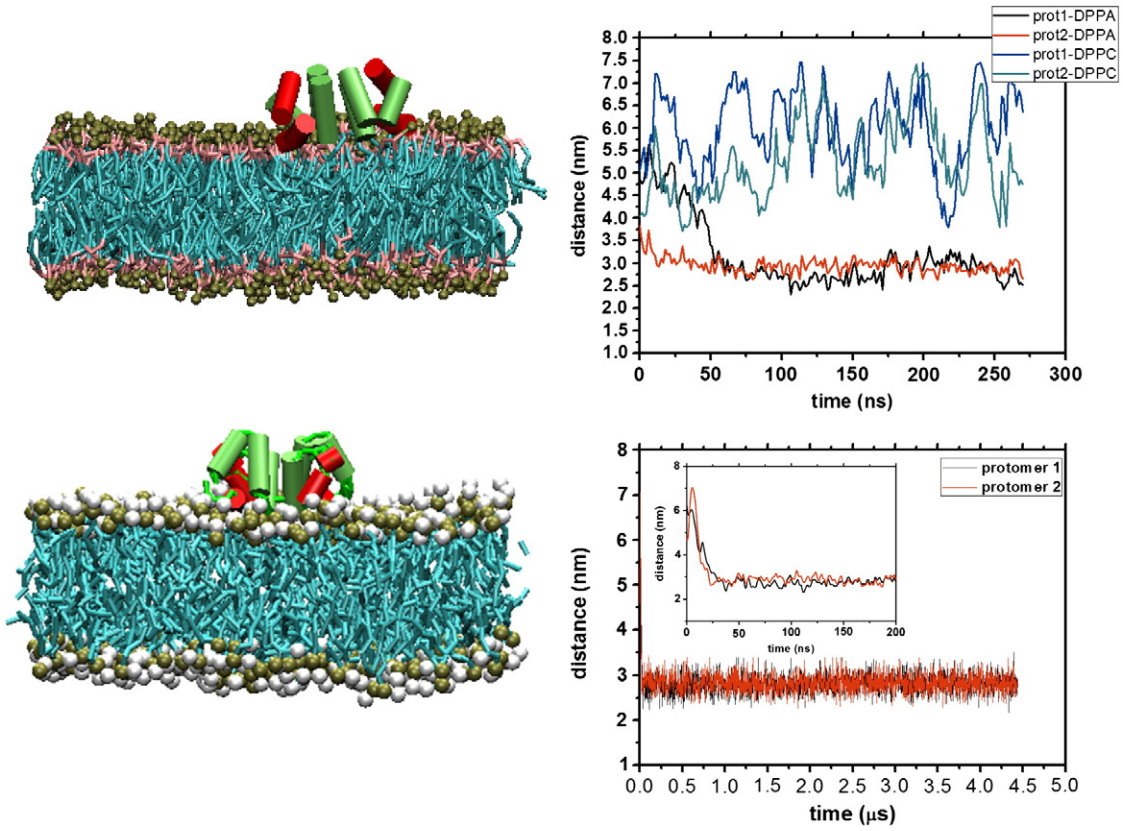

Fig. 4. Binding of dimeric form I. Upper left: AS-48 dimer bound to a DPPA bilayer. Peptides are represented as in Fig. 3. The phosphate polar head particles of each lipid appear as gold balls and hydrophobic lipid chains as blue lines. Solvent particles are omitted. Upper right: distances between the centre of mass of each AS-48 protomer and the bilayer centre for both DPPA and DPPC lipid systems. Lower left: AS-48 dimer bound to a DPPG bilayer. Lower right: distances between the centre of mass of each AS-48 protomer and the bilayer centre for the DPPG system.

some particular configuration, as is likely the case for surface binding structures.

3.3. Pore formation

Considering the experimental information to date, pore formation should take place in a time scale of milliseconds [28]. We therefore ran self-assembly computational simulations of the AS-48 peptide in a DPPA/solvent mixture [57]. This kind of simulation has been used by others to explore peptide–membrane interactions by coarse-grained methods [48]. We simulated a system consisting of four separate bacteriocin protomers immersed in a box containing 200 DPPA molecules together with 5000 water particles and a sufficient number of counterions to generate a neutral system. The system was energy minimized and equilibrated with position restraints on the protomers. Simulations were then performed for at least another 2.7 μs using NPT molecular dynamics as described in the Computation methods section. In this case, isotropic pressure coupling was performed with a 1 atm reference pressure and compressibility of 4.6×10^{-5} bar^{-1}. The simulation protocol was repeated for different starting configurations produced by randomly assigning different locations and orientations to the peptide molecules in the box. In total, 15 self-assembly simulations were performed. The pore structures formed remained stable during the last 1 μs of simulation.

All self-assembly simulations yielded a bilayer structure in which the AS-48 protomers were fully embedded. Protomers were generally aligned such that hydrophobic helices H1 to H3 could interact with the DPPA acyl chains. The charged helices H4 and H5 were also observed in the bilayer. These charged helices showed two different alignments depending on whether they interacted with other protomer helices or with lipid bilayer head groups.

Interactions between the protomer's hydrophobic moieties observed for the dimer partially shifted to interactions with lipid acyl chains. In turn, charged amino acid-rich helices 4 and 5 in the different protomers either interacted amongst each other or with the lipid phosphate particles. Fig. S4 provides a minimum inter-residue distance map for the four peptides of a selected self-assembly simulation. Contrasting with the situation for the dimer in solution, some interaction between charged residues of different peptides was observed, e.g., between the first and fifth protomers. In addition, hydrophobic interactions amongst peptides were weaker (compare Figs. S2 and S4).

In 9 of the 15 simulated systems, direct interaction was detected between helices 4 and 5 and the lipid phosphate groups throughout the bilayer interior, dragging water particles and giving rise to positive curvature of the lipid layer. Moreover, this embedding of the particle in the membrane provoked the formation of toroidal-like pores of variable dimension (see Fig. 5). These toroidal pores resemble those proposed by Zhao et al. for their "leaky slit" model [58]. Pore structure was also in line with the model first anticipated by Ludtke for magainin [59] and the description of these pores by Marrink and co-workers as disordered structures [9,16]. Pore structure was very stable during the last microsecond of simulation, with the three hydrophobic helices interacting with the lipid tails and the charged residues of helices 4 and 5, either on the bilayer surface or in its interior facing the charged phosphate particles making up the toroidal lipid structure.

One of these simulations gave rise to a structure that could be assigned to a protein fibril. In this simulation, the four AS-48 protomers form a linear, amphipathic array inside the bilayer interior. A fracture is produced in the bilayer in a manner equivalent to that proposed for the "leaky slit" model discussed in reference [58]. The resulting linear arrangement of the protomers is graphically shown in Fig. 6. It can be

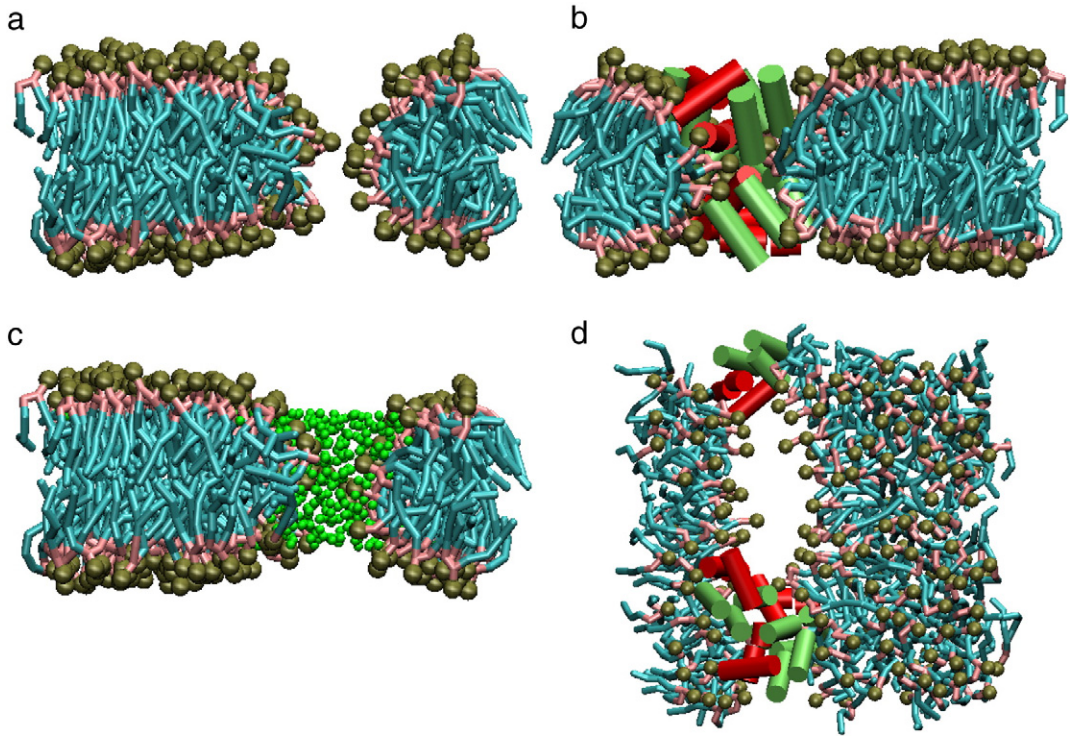

Fig. 5. Different views of the "toroidal" pore geometry produced after 2.7 μs of simulation. a: DPPA particles. b: DPPA + AS-48 protomers. c: DPPA + water particles (shown as small green balls) penetrating the bilayer. d: View across the normal to the bilayer of DPPA + AS-48 protomers. AS-48 hydrophobic and charged helices are represented as green and red cylinders, respectively.

seen that the hydrophobic helices (green cylinders in the figure) interact with the hydrophobic lipid chains in a fraction of the bilayer. On the other hand, the charged helices (red cylinders in the figure) force the positive curvature of the lipid bilayer through electrostatic interaction with charged phosphate particles, and these give rise to a toroidal pore. The curved bilayer surface can be seen in Fig. 6a, and the linear arrangement of the AS-48 protomers in Fig. 6d.

The charged residues effectively penetrate the bilayer interior. Positively charged LYS and ARG amino acids drag the negative phosphate lipid particles, which form a lipid surface with a positive

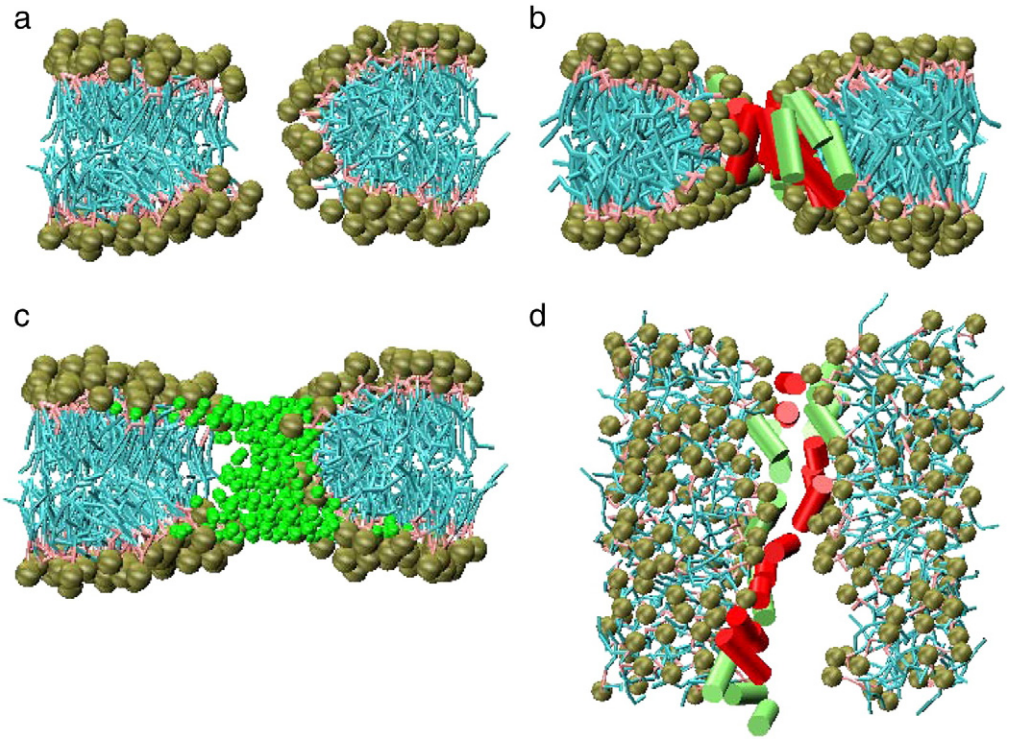

Fig. 6. Different views of the fibril-like pore geometry produced after at 2.7 μs simulation. a: DPPA particles. b: DPPA + AS-48 protomers. c: DPPA + water particles (shown as small green balls) penetrating the bilayer. d: View across the normal to the bilayer of DPPA + AS-48 protomers. AS-48 hydrophobic and charged helices are represented as green and red cylinders, respectively.

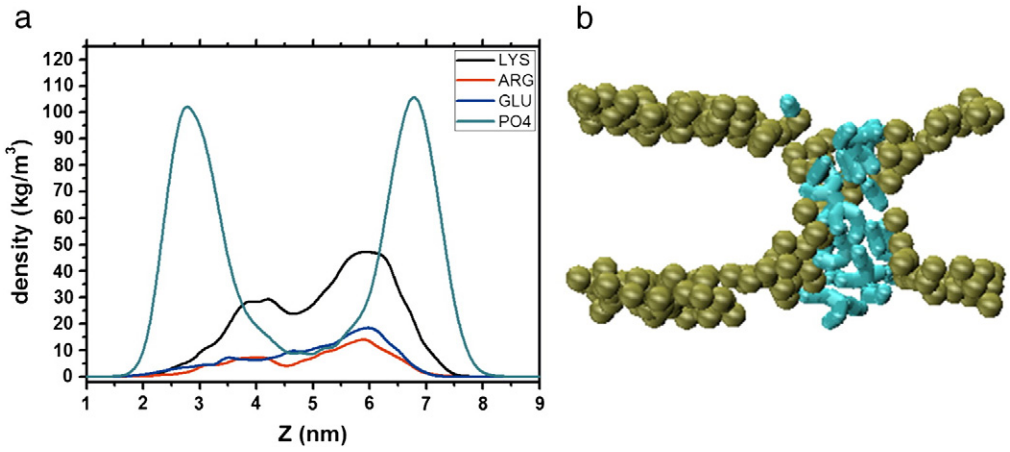

Fig. 7. Specific interactions between AS-48 protomers and DPPA. a: Density profiles for PO_4 particles and charged LYS, ARG and GLU residues. b: Structure representation of a final simulation snapshot showing the distribution of LYS residues (cyan bonds) and PO_4 lipid particles (gold balls).

curvature. Fig. 7a shows a density profile for the phosphate particles and charged residues along the bilayer axis. Around the bilayer mid-point, densities for the lipid head particles were not zero. This is typical of phosphate particles inside a bilayer. In addition, the density of charged residues, particularly LYS, occurs in the membrane interior. Fig. 7b shows a detailed picture of the LYS residues facing the phosphate particles to create a positive-curvature lipid surface, compatible with the presence of a large pore.

Another structural arrangement found for the pore formation process is that shown in Fig. 8. In this case, most of the charged residues in the H4 and H5 helices of different protomers are oriented towards the centre of a pseudo cylindrical hole formed by the proteins, which are in turn shielded from the lipid hydrophobic phase by helices 1 to 3 (see Fig. 8a).

The pore seems to be narrower in this second structure type (closed pore). In our simulations, the hydrophobic helices of each protomer interact with the DPPA tails such that charged helices 4 and 5 sometimes point to the pore interior while others occur at the lipid surface and interact with the water phase (see Fig. 8b). Only a few phosphate particles were dragged to the bilayer interior, as observed for the toroidal pores (see Fig. 8c).

Table 1 provides parameters associated with the different pore types for each self-assembly simulation: estimated pore diameter and the density of phosphate particles inside the hydrophilic bilayer zone. As described earlier, pore type was defined as “toroidal” or “closed”. Pore diameter was estimated from the density profile of water molecules through the bilayer. The formation of a pore implies that water penetrates the bilayer's hydrophobic core in a quantity directly proportional to pore size. This pore size can be estimated from the ratio of the water density values for the hydrophobic region relative to bulk density values. The following equation gives an estimate of pore radius assuming the cylindrical geometry of a pore:

$$(\rho_w/\rho_{bulk}) = \left(\pi \langle r \rangle^2 / b_x b_y\right) \quad (1)$$

where b_x and b_y are the box dimensions in the membrane plane. The average radius ($\langle r \rangle$) is calculated from all contributions to water density inside the hydrophobic core region (ρ_w) spanned by the bilayer's acyl chains. For example, in Fig. 9, density profiles for water, hydrophobic and phosphate lipid particles are provided for the last μs of a particular simulation yielding a closed pore. The hydrophobic core region of the lipid bilayer can be assumed to be located between 3.9 and 5.4 nm. The average ρ_w for this region is then calculated. The mean water density value for the bulk (ρ_{bulk}) can be taken as an approximate value for water density just above and below the membrane bilayer (0–2 nm and 7–9.5 nm in this example). In this hydrophobic region, average PO_4 density can also be determined. These values give information about the relative quantity of phosphate particles protruding into the lipid bilayer to form a toroidal surface of positive curvature (see Fig. 5).

Table 1 indicates that pore radius is 0.6 to 1.0 nm for a closed pore and 1.5 to 3.0 nm for a toroidal pore. It can be observed that for phosphate particles in hydrophobic regions, closed pores show

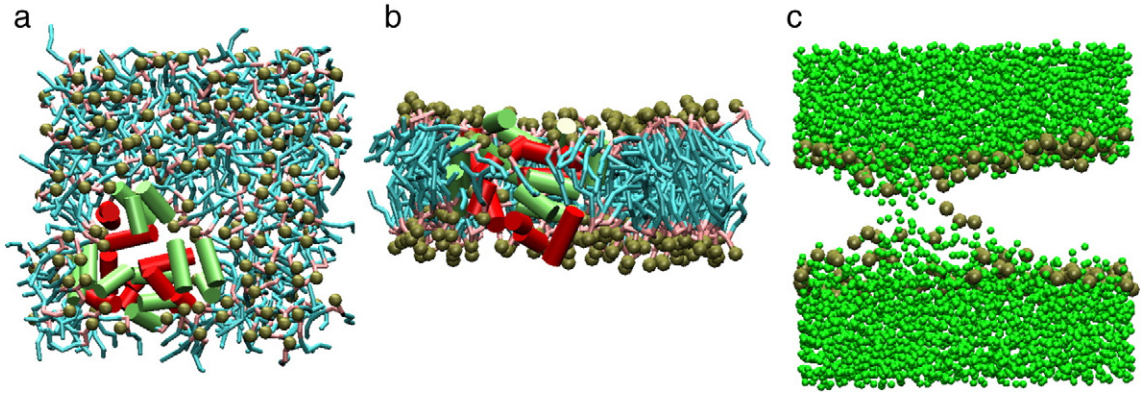

Fig. 8. Closed pore formation. a: Normal to the bilayer view of the pore formed by four AS-48 protomers. Peptides and lipids are represented as in the remaining figs. b: Lateral view. c: View across the bilayer of the pore formed showing only water particles (in green) and PO_4 particles (in gold) penetrating the bilayer interior.

Table 1
Pore characteristics associated to each self-assembly simulation.

Simulation #	Pore type	Pore radius (nm)	PO_4 density inside pore (kg/m^3)
1	Toroidal	1.7 ± 0.3	10.9 ± 0.9
2	Closed	0.9 ± 0.1	5.8 ± 0.5
3	Toroidal	1.4 ± 0.1	6.7 ± 0.5
4	Toroidal	2.0 ± 0.1	14.6 ± 0.7
5	Toroidal	2.1 ± 0.1	15.8 ± 0.4
6	Closed	0.7 ± 0.1	2.2 ± 0.3
7	Toroidal	1.7 ± 0.2	7.3 ± 0.3
8	Closed	1.0 ± 0.1	4.9 ± 0.2
9	Toroidal	1.6 ± 0.1	12.5 ± 0.9
10	Closed	0.9 ± 0.2	7.3 ± 0.3
11	Closed	0.7 ± 0.1	4.9 ± 0.3
12	Toroidal	2.9 ± 0.3	18.7 ± 0.3
13	Toroidal	2.8 ± 0.4	22.0 ± 0.8
14	Closed	0.6 ± 0.1	4.5 ± 0.2
15	Toroidal	2.9 ± 0.3	28.2 ± 0.9
Average	Toroidal	2.1 ± 0.6	15.2 ± 6.9
Average	Closed	0.8 ± 0.2	4.9 ± 1.7

PO_4 averaged densities of 4.9 ± 1.7 kg/m^3, and toroidal pores of 15.2 ± 7.0 kg/m^3.

In both pore types, the hydrophobic helices of each protomer span the entire width of the bilayer. Bilayer width is around 1 nm more than the size of the AS-48 hydrophobic helix package, so a hydrophobic mismatch is expected. This mismatch can be resolved by bending the phosphate layer to interact more effectively with the charged residues of the peptides (see Fig. 5).

4. Conclusions

Our coarse-grained simulations showed good agreement with experimental data reported for the bactericidal activity of peptide AS-48. The stability of the dimer in aqueous solution was confirmed in 3 μs simulations in which the hydrophobic core was shielding by charged helices 4 and 5, thus preserving the so-called dimeric form I indicated by crystallography and NMR experiments.

In solution, the dimer binds to anionic DPPA and DPPG lipid bilayers but not to the zwitterionic DPPC bilayer. This is consistent with the experimental observation that this peptide shows specificity towards bacterial membranes, which contain high proportions of anionic lipids.

Through self-assembly simulations of systems comprised of the AS-48 protomers, DPPA molecules, water particles and the corresponding number of counterions, the capacity of this bacteriocin to induce the formation of stable pores was examined. Our findings indicate that the pore formation process takes place in a millisecond to second timescale, far beyond predictions so far using coarse-grained models. The purpose of self-assembly simulation is to yield stable structures comprised of the assembled lipid bilayer and trans-membrane protein as a shortcut to obtain the final inserted structures. Two types of pore were produced. The first type was a small pore of around 1 nm radius, which is in close agreement with experimental estimates. This pore is formed by at least three protomers oriented in such a way that several charged residues point to the pore centre while they are shielded from the lipid hydrocarbon tails by hydrophobic helices with additional lipid phosphate groups lined up along the pore margin. The second pore type was a larger toroidal pore of variable dimension formed by dragging of phosphate lipid groups towards the bilayer interior due to interactions with charged protein residues. The resulting structure is mostly in agreement with the "leaky slit" model.

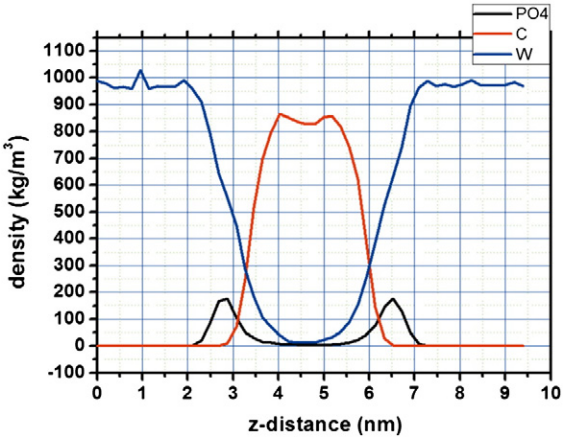

Fig. 9. Density profiles across the normal to the bilayer for the water, phosphate and acyl particles of an average "closed" pore structure for the last 1 μs of simulation.

The coarse-grained simulations presented allow the interpretation of several experimental data and provide a model for the type of pore that this interesting bacteriocin is able to generate.

Supplementary data to this article can be found online at http://dx.doi.org/10.1016/j.bbamem.2013.05.036.

Acknowledgements

This work was performed under the project HPC-EUROPA2 (project number: 228398) with support of the European Commission – Capacities Area – Research Infrastructures. The study was funded by the CICYT (MAT2009-12364 and MAT2012-36341 projects) and a European grant (FP7-PEOPLE-2009-IEF-254559) awarded to M.M. J.R. received financial support through a Ramon y Cajal program contract RYC-2011-09585. The authors thank Prof. Marrink for help in the different work stages and "SGAI-CSIC" for technical support during the simulations.

References

[1] L. Chen, L. Gao, W. Fang, L. Golubovic, How the antimicrobial peptides kill bacteria: computational physics insights, CiCP 11 (2012) 709–725.
[2] X. Chen, Z. Chen, Sfg studies on interactions between antimicrobial peptides and supported lipid bilayers, Biochim. Biophys. Acta-Biomembr. 1758 (2006) 1257–1273.
[3] R.M. Epand, R.F. Epand, Bacterial membrane lipids in the action of antimicrobial agents, J. Pept. Sci. 17 (2011) 298–305.
[4] C.D. Fjell, J.A. Hiss, R.E.W. Hancock, G. Schneider, Designing antimicrobial peptides: form follows function, Nat. Rev. Drug Discov. 11 (2012) 37–51.
[5] J.N. Horn, J.D. Sengillo, D.J. Lin, T.D. Romo, A. Grossfield, Characterization of a potent antimicrobial lipopeptide via coarse-graining molecular dynamics, Biochim. Biophys. Acta-Biomembr. 1818 (2012) 212–218.
[6] A. Khalfa, M. Tarek, On the antibacterial action of cyclic peptides: insights from coarse-graining md simulations, J. Phys. Chem. B 114 (2010) 2676–2684.
[7] P. La Rocca, P.C. Biggin, D.P. Tieleman, M.S.P. Sansom, Simulation studies of the interaction of antimicrobial peptides and lipid bilayers, Biochim. Biophys. Acta-Biomembr. 1462 (1999) 185–200.
[8] M.D. Lad, F. Birembaut, L.A. Clifton, R.A. Frazier, J.R.P. Webster, R.J. Green, Antimicrobial peptide–lipid binding interactions and binding selectivity, Biophys. J. 92 (2007) 3575–3586.
[9] H. Leontiadou, A.E. Mark, S.J. Marrink, Antimicrobial peptides in action, J. Am. Chem. Soc. 128 (2006) 12156–12161.
[10] S.J. Marrink, A.H. de Vries, D.P. Tieleman, Lipids on the move: simulations of membrane pores, domains, stalks and curves, Biochim. Biophys. Acta-Biomembr. 1788 (2009) 149–168.
[11] E. Matyus, C. Kandt, D.P. Tieleman, Computer simulation of antimicrobial peptides, Curr. Med. Chem. 14 (2007) 2789–2798.
[12] M.N. Melo, R. Ferre, M.A.R.B. Castanho, Opinion antimicrobial peptides: linking partition, activity and high membrane-bound concentrations, Nat. Rev. Microbiol. 7 (2009) 245–250.
[13] J.T. Mika, G. Moiset, A.D. Cirac, L. Feliu, E. Bardaji, M. Planas, D. Sengupta, S.J. Marrink, B. Poolman, Structural basis for the enhanced activity of cyclic antimicrobial peptides: the case of bpc194, Biochim. Biophys. Acta-Biomembr. 1808 (2011) 2197–2205.
[14] M. Pasupuleti, A. Schmidtchen, M. Malmsten, Antimicrobial peptides: key components of the innate immune system, Crit. Rev. Biotechnol. 32 (2012) 143–171.
[15] K.P. Santo, M.L. Berkowitz, Difference between magainin-2 and melittin assemblies in phosphatidylcholine bilayers: results from coarse-graining simulations, J. Phys. Chem. B 116 (2012) 3021–3030.
[16] D. Sengupta, H. Leontiadou, A.E. Mark, S.-J. Marrink, Toroidal pores formed by antimicrobial peptides show significant disorder, Biochim. Biophys. Acta-Biomembr. 1778 (2008) 2308–2317.

[17] C.I.E. von Deuster, V. Knecht, Competing interactions for antimicrobial selectivity based on charge complementarity, Biochim. Biophys. Acta-Biomembr. 1808 (2011) 2867–2876.
[18] W.C. Wimley, Describing the mechanism of antimicrobial peptide action with the interfacial activity model, ACS Chem. Biol. 5 (2010) 905–917.
[19] M. Mihajlovic, T. Lazaridis, Charge distribution and imperfect amphipathicity affect pore formation by antimicrobial peptides, Biochim. Biophys. Acta-Biomembr. 1818 (2012) 1274–1283.
[20] Y. Wang, D.E. Schlamadinger, J.E. Kim, J.A. McCammon, Comparative molecular dynamics simulations of the antimicrobial peptide cm15 in model lipid bilayers, Biochim. Biophys. Acta-Biomembr. 1818 (2012) 1402–1409.
[21] S. Qian, W. Wang, L. Yang, H.W. Huang, Structure of the alamethicin pore reconstructed by X-ray diffraction analysis, Biophys. J. 94 (2008) 3512–3522.
[22] A. Galvez, M. Maqueda, M. Martinezbueno, E. Valdivia, Bactericidal and bacteriolytic action of peptide antibiotic AS-48 against gram-positive and gram-negative bacteria and other organisms, Res. Microbiol. 140 (1989) 57–68.
[23] A. Galvez, M. Maqueda, E. Valdivia, A. Quesada, E. Montoya, Characterization and partial-purification of a broad-spectrum antibiotic AS-48 produced by streptococcus-faecalis, Can. J. Microbiol. 32 (1986) 765–771.
[24] B. Samyn, M. Martinezbueno, B. Devreese, M. Maqueda, A. Galvez, E. Valdivia, J. Coyette, J. Vanbeeumen, The cyclic structure of the enterococcal peptide antibiotic AS-48, FEBS Lett. 352 (1994) 87–90.
[25] E.S. Cobos, V.V. Filimonov, A. Galvez, N. Maqueda, E. Valdivia, J.C. Martinez, P.L. Mateo, AS-48: a circular protein with an extremely stable globular structure, FEBS Lett. 505 (2001) 379–382.
[26] C. Gonzalez, G.M. Langdon, M. Bruix, A. Galvez, E. Valdivia, M. Maqueda, M. Rico, Bacteriocin AS-48, a microbial cyclic polypeptide structurally and functionally related to mammalian nk-lysin, Proc. Natl. Acad. Sci. U. S. A. 97 (2000) 11221–11226.
[27] M.J. Sanchez-Barrena, M. Martinez-Ripoll, A. Galvez, E. Valdivia, M. Maqueda, V. Cruz, A. Albert, Structure of bacteriocin AS-48: from soluble state to membrane bound state, J. Mol. Biol. 334 (2003) 541–549.
[28] A. Galvez, M. Maqueda, M. Martinezbueno, E. Valdivia, Permeation of bacterial-cells, permeation of cytoplasmic and artificial membrane-vesicles, and channel formation on lipid bilayers by peptide antibiotic AS-48, J. Bacteriol. 173 (1991) 886–892.
[29] M. Maqueda, A. Galvez, M.M. Bueno, M.J. Sanchez-Barrena, C. Gonzalez, A. Albert, M. Rico, E. Valdivia, Peptide AS-48: prototype of a new class of cyclic bacteriocins, Curr. Protein Pept. Sci. 5 (2004) 399–416.
[30] H. Abriouel, M. Maqueda, A. Galvez, M. Martinez-Bueno, E. Valdivia, Inhibition of bacterial growth, enterotoxin production, and spore outgrowth in strains of bacillus cereus by bacteriocin AS-48, Appl. Environ. Microbiol. 68 (2002) 1473–1477.
[31] J.D. Gehman, F. Luc, K. Hall, T.-H. Lee, M.P. Boland, T.L. Pukala, J.H. Bowie, M.-I. Aguilar, F. Separovic, Effect of antimicrobial peptides from Australian tree frogs on anionic phospholipid membranes, Biochemistry 47 (2008) 8557–8565.
[32] F. Jean-Francois, S. Castano, B. Desbat, B. Odaert, M. Roux, M.-H. Metz-Boutigue, E.J. Dufourc, Aggregation of cateslytin beta-sheets on negatively charged lipids promotes rigid membrane domains. A new mode of action for antimicrobial peptides? Biochemistry 47 (2008) 6394–6402.
[33] K. Matsuzaki, K. Sugishita, M. Harada, N. Fujii, K. Miyajima, Interactions of an antimicrobial peptide, magainin 2, with outer and inner membranes of gram-negative bacteria, Biochim. Biophys. Acta-Biomembr. 1327 (1997) 119–130.
[34] P.F. Devaux, Static and dynamic lipid asymmetry in cell-membranes, Biochemistry 30 (1991) 1163–1173.
[35] W. Dowhan, Molecular basis for membrane phospholipid diversity: why are there so many lipids? Annu. Rev. Biochem. 66 (1997) 199–232.
[36] H. Abriouel, J. Sanchez-Gonzalez, M. Maqueda, A. Galvez, E. Valdivia, M.J. Galvez-Ruiz, Monolayer characteristics of bacteriocin AS-48, ph effect and interactions with dipalmitoyl phosphatidic acid at the air–water interface, J. Colloid Interface Sci. 233 (2001) 306–312.
[37] M. Sanchez-Hidalgo, A.M. Fernandez-Escamilla, M. Martinez-Bueno, E. Valdivia, L. Serrano, M. Maqueda, Conformational stability and activity of circular enterocin AS-48 derivatives, Protein Pept. Lett. 17 (2010) 708–714.
[38] M. Montalban-Lopez, M. Martinez-Bueno, E. Valdivia, M. Maqueda, Expression of linear permutated variants from circular enterocin AS-48, Biochimie 93 (2011) 549–555.
[39] M. Sanchez-Hidalgo, A. Ma Fernandez-Escamilla, M. Martinez-Bueno, E. Valdivia, L. Serrano, M. Maqueda, Conformational stability and activity of circular enterocin AS-48 derivatives, Protein Pept. Lett. 17 (2010) 708–714.
[40] M. Sanchez-Hidalgo, M. Martinez-Bueno, A.M. Fernandez-Escamilla, E. Valdivia, L. Serrano, M. Maqueda, Effect of replacing glutamic residues upon the biological activity and stability of the circular enterocin AS-48, J. Antimicrob. Chemother. 61 (2008) 1256–1265.
[41] M. Sanchez-Hidalgo, M. Montalban-Lopez, R. Cebrian, E. Valdivia, M. Martinez-Bueno, M. Maqueda, AS-48 bacteriocin: close to perfection, Cell. Mol. Life Sci. 68 (2011) 2845–2857.
[42] S.V. Bennun, M.I. Hoopes, C. Xing, R. Faller, Coarse-graining modeling of lipids, Chem. Phys. Lipids 159 (2009) 59–66.
[43] A.A. Gurtovenko, J. Anwar, I. Vattulainen, Defect-mediated trafficking across cell membranes: insights from in silico modeling, Chem. Rev. 110 (2010) 6077–6103.
[44] S.O. Nielsen, C.F. Lopez, G. Srinivas, M.L. Klein, Coarse grain models and the computer simulation of soft materials, J. Phys. Condens. Matter 16 (2004) R481–R512.
[45] A.J. Rzepiela, D. Sengupta, N. Goga, S.J. Marrink, Membrane poration by antimicrobial peptides combining atomistic and coarse-graining descriptions, Faraday Discuss. 144 (2010) 431–443.
[46] M.S.P. Sansom, I.H. Shrivastava, J.N. Bright, J. Tate, C.E. Capener, P.C. Biggin, Potassium channels: structures, models, simulations, Biochim. Biophys. Acta-Biomembr. 1565 (2002) 294–307.
[47] N. Sapay, D.P. Tieleman, Molecular dynamics simulation of lipid–protein interactions, in: S.E. Feller (Ed.), Computational Modeling of Membrane Bilayers, vol. 60, 2008, pp. 111–130.
[48] B.A. Hall, A.P. Chetwynd, M.S.P. Sansom, Exploring peptide–membrane interactions with coarse-graining md simulations, Biophys. J. 100 (2011) 1940–1948.
[49] W.F.D. Bennett, D.P. Tieleman, Water defect and pore formation in atomistic and coarse-graining lipid membranes: pushing the limits of coarse graining, J. Chem. Theory Comput. 7 (2011) 2981–2988.
[50] H. Hwang, G.C. Schatz, M.A. Ratner, Coarse-graining molecular dynamics study of cyclic peptide nanotube insertion into a lipid bilayer, J. Phys. Chem. A 113 (2009) 4780–4787.
[51] S.J. Marrink, H.J. Risselada, S. Yefimov, D.P. Tieleman, A.H. de Vries, The MARTINI force field: coarse graining model for biomolecular simulations, J. Phys. Chem. B 111 (2007) 7812–7824.
[52] L. Monticelli, S.K. Kandasamy, X. Periole, R.G. Larson, D.P. Tieleman, S.-J. Marrink, The MARTINI coarse-graining force field: extension to proteins, J. Chem. Theory Comput. 4 (2008) 819–834.
[53] H.J.C. Berendsen, J.P.M. Postma, W.F. Vangunsteren, A. Dinola, J.R. Haak, Molecular-dynamics with coupling to an external bath, J. Chem. Phys. 81 (1984) 3684–3690.
[54] B. Hess, C. Kutzner, D. van der Spoel, E. Lindahl, Gromacs 4: algorithms for highly efficient, load-balanced, and scalable molecular simulation, J. Chem. Theory Comput. 4 (2008) 435–447.
[55] X. Periole, M. Cavalli, S.-J. Marrink, M.A. Ceruso, Combining an elastic network with a coarse-graining molecular force field: structure, dynamics, and intermolecular recognition, J. Chem. Theory Comput. 5 (2009) 2531–2543.
[56] S.O. Yesylevskyy, L.V. Schafer, D. Sengupta, S.J. Marrink, Polarizable water model for the coarse-graining MARTINI force field, PLoS Comp. Biol. 6 (2010).
[57] W. Shinoda, R. DeVane, M.L. Klein, Computer simulation studies of self-assembling macromolecules, Curr. Opin. Struct. Biol. 22 (2012) 175–186.
[58] H. Zhao, R. Sood, A. Jutila, S. Bose, G. Fimland, J. Nissen-Meyer, P.K.J. Kinnunen, Interaction of the antimicrobial peptide pheromone plantaricin a with model membranes: implications for a novel mechanism of action, Biochim. Biophys. Acta-Biomembr. 1758 (2006) 1461–1474.
[59] S.J. Ludtke, K. He, W.T. Heller, T.A. Harroun, L. Yang, H.W. Huang, Membrane pores induced by magainin, Biochemistry 35 (1996) 13723–13728.